Collimated gamma-beams with high peak flux driven by laser-accelerated electrons

Lulin Fan[1,2,†], Tongjun Xu[1,†✉], Shun Li[1], Zhangli Xu[3], Jiancai Xu[1], Jianqiang Zhu[1], Baifei Shen[1,3], Liangliang Ji[1✉]

1State Key Laboratory of High Field Laser Physics, Shanghai Institute of Optics and Fine Mechanics, Chinese Academy of Sciences

2University of Chinese Academy of Sciences, Beijing 100049, China

3Shanghai Normal University, Shanghai 200234, China

Abstract

Laser-accelerated electrons are promising in producing gamma-photon beams of high peak flux for study of nuclear photonics, obtaining copious positrons and exploring photon-photon interaction in vacuum. We report on experimental generation of brilliant gamma-ray beams with not only high photon yield but also low divergence, based on picosecond laser-accelerated electrons. The 120J 1ps laser pulse drives self-modulated wakefield in a high-density gas jet and generates tens-of-MeV electrons with 26nC and divergence as small as 1.51°. These collimated electrons produce gamma-ray photons through Bremsstrahlung when transversing a high-Z solid target. We design a high-energy-resolution Compton-scattering spectrometer (CSS) and find that a total photon number of 2.2×10^9 is captured within an acceptance angle of $1.1°$ for photon energies up to $16\,\mathrm{MeV}$. Comparison between the experimental results and Monte-Carlo simulations illustrates that the photon beam inherits the small divergence from electrons, corresponding to a total photon number

† These authors contributed equally to this work.
✉ email: tjxu@siom.ac.cn; jill@siom.ac.cn.

This peer-reviewed article has been accepted for publication but not yet copyedited or typeset, and so may be subject to change during the production process. The article is considered published and may be cited using its DOI.

10.1017/hpl.2023.25

2.2×10^{11} and a divergence $7.73°$.

Keywords: gamma-ray beam, laser-electron acceleration, Bremsstrahlung, Compton-scattering spectrometer

1. Introduction

In recent years, laser-driven particle sources such as electrons[1], ions[2] and neutrons[3] have been greatly developed due to the promising applications in high energy density physics, nuclear physics, cancer therapy treatment etc. Based on laser-accelerated electrons, gamma-ray radiations are also gaining rising interests for the ultra-high peak brilliance, short pulse duration and small beam size[4-7]. Such compact gamma-ray sources could pave the way for nuclear photonics, producing ultrashort neutron sources and medical isotopes[8], and radiography. Particularly, the small beam size and large peak flux of the laser-generated gamma-ray sources can greatly improve the contrast and spatial resolution for nondestructive radiography compared to other approaches[9]. In strong-field quantum-electrodynamics, a promising approach to observe the Breit-Wheeler electron-positron pair production[10] in the linear or nonlinear regime is to collide laser-driven gamma photons with superintense lasers[11], X-ray radiations[12] or with each other. This requires the gamma beams to be collimated, guaranteeing high photon density in the collision region.

There are three main mechanisms to generate gamma-ray beams based on laser-driven energetic electrons in experiment: betatron radition[13], inverse Compton scattering (ICS)[14, 15] and bremsstrahlung radiation[4, 5, 16, 17]. In general, Betatron radiation produces gamma-rays with photon energies from hundreds of keV to MeV when electrons oscillate in the laser-driven plasma bubble field. In ICS, the number of photons obtained by laser photons scattered by high energy electrons is usually at 10^7 level[18], with photon energies up to several tens of MeV and good beam collimation. On the other hand, copious gamma-photons can be produced when energetic electrons collide with high atomic-number nuclei through Bremsstrahlung radiation. In this case, the maximum energy of the gamma-photon is comparable to the maximum electron energy. It is advantageous on producing large photon numbers, up to 3.2×10^{10} by femtosecond

https://doi.org/10.1017/hpl.2023.25 Published online by Cambridge University Press

laser[17] .

A key to increase the photon yield in Bremsstrahlung is enhancing the number of relativistic electrons in laser-plasma accelerations. For instance[16], using picosecond laser pulses of relatively high pulse energy, plasma wakefield acceleration in the self-modulated regime produces 7.5 nC electrons hence inducing photon number of 10^9 Photons $\mathrm{keV}^{-1}\,Sr^{-1}$. However, the divergence of bremsstrahlung gamma-ray beams is usually quite large (~several tens of degree)[17] because of the scattering by the nucleus coulomb field.

In this work, to obtain high yield low divergence gamma sources, we first produce a collimated high charge electron beam through picosecond laser-driven self-modulated wakefield acceleration (SM-LWFA). Then it is sent to a high-Z target. The bremsstrahlung gamma-ray photons are measured with a high-resolution Compton-scattering spectrometer (CSS). The latter contains a gradual magnetic field to improve the energy resolution. The measured spectra are reproduced with GEANT4 simulations, suggesting a total photon number of 2.2×10^{11} gamma-photons (>0.3MeV) within a divergence angle of $7.73°$. Such gamma-photons are advantageous in radiography, exploring nuclear photonics, strong-field QED physics etc.

2. Experimental setup

The experiment was carried out in the SG-II UP picosecond experimental platform[19] at Shanghai Institute of Optics and Fine Mechanics(SIOM). The schematic diagram of the experiment is shown in Fig. 1. A linearly polarized laser pulse with a pulse duration of $\tau_p = 1\mathrm{ps}$, a center wavelength of 1053 nm, and an energy of $120\,\mathrm{J}$ was focused $600\,\mu\mathrm{m}$ above a pulsed nozzle which is employed to produce a high-density argon gas jet by an $f/2.8$ off-axis parabolic mirror. The focal spot has a full width at half maximum (FWHM) of $35\,\mu\mathrm{m}$, reaching peak intensity of $3.1 \times 10^{18}\ \mathrm{W/cm^2}$. On-target laser field corresponds to a normalized laser amplitude $a \approx 2.3$, where $a = eE/m\omega c$, e and m are the electron charge and mass, E is the electric field, ω is the laser frequency, and c is the speed of light in vacuum, respectively. The back pressure of the argon gas target in the experiment was $17 - 30$ bar, and optical interferometry of the laser-gas jet interaction indicated that the electron density reached a near critical density region $2{\sim}4 \times 10^{20}\,\mathrm{cm^{-3}}$, corresponding to a plasma wavelength $\lambda_p \approx 1.9\,\mu\mathrm{m}$. A $2\,\mathrm{mm}$ thick lead target was placed $2\,\mathrm{mm}$ behind the gas jet. When the laser-accelerated energetic electrons pass through the solid target, they are scattered by the nuclei and emit photons through bremsstrahlung.

https://doi.org/10.1017/hpl.2023.25 Published online by Cambridge University Press

Electron-positron pair creation through Bethe-Heitler process[20] also occurs during the interaction process when the emitted photons further interact with nuclei. An electron-positron spectrometer (EPS) with the magnetic field of $B = 0.8\mathrm{T}$ was added $220\,\mathrm{mm}$ behind the lead target to deflect the positrons and electrons and measure their energy spectra, which had an acceptance divergence angle of $2.86°$. We chose Fuji BAS-SR (or BAS-TR) image plates (IPs) as the recording detector. The IPs was scanned using a GE Typhoon 7000 flatbed image plate scanner[21].

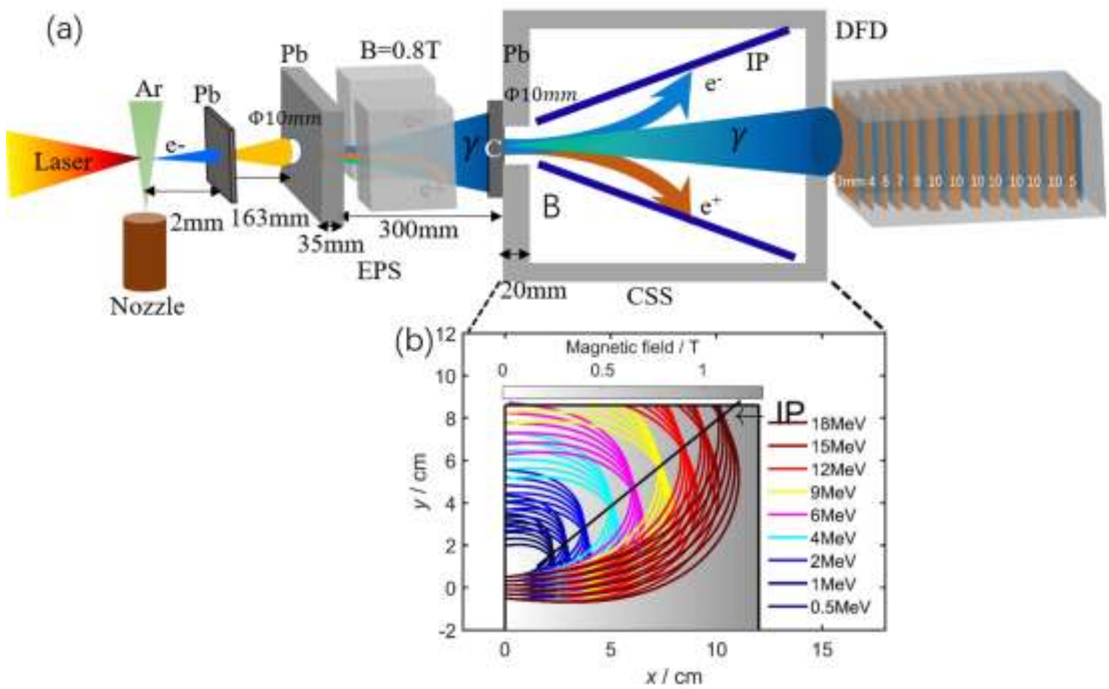

FIG.1. Schematic of experimental setup. (a) A laser pulse propagates through an argon gas target, energetic electrons are generated and collide with the 2mm lead target located 2mm behind the gas target to generate gamma-ray beams. An electron-positron spectrometer (EPS) with an aperture of 10 mm located $220\,\mathrm{mm}$ behind the lead target with an acceptance divergence angle of $2.86°$ is added to deflect the positrons and electrons and measure their energy spectra. The gamma-ray beam spectra are measured with a typical differential filtering detector (DFD) and a Compton-scattering spectrometer (CSS) with a gradual magnet, which increases linearly along the laser direction and fills the whole spectrometer. The converter target in the CSS is carbon with thickness of 2 mm. The CSS and differential filtering detector are added $500\,\mathrm{mm}$ behind the lead target, which has an acceptance divergence angle of $1.1°$. (b) Trajectories of the converted electron beams dispersed in the gradual magnetic field. There trajectories represent incident electron beams with energies 0.5 MeV-18 MeV. The converter electrons enter the magnetic field with different transverse positions of $[-5, 5]$mm, and different angles of [-5°, 5°].

https://doi.org/10.1017/hpl.2023.25 Published online by Cambridge University Press

One key aspect of our experiments is the measurement of the gamma-ray spectrum. Gamma-ray beams driven by laser-accelerated electrons are of short pulse duration, comparable to that of the laser pulse (~1ps here). Conventional scintillation and semiconductor detectors are not applicable to resolve the energy spectrum of the gamma-ray flash since all photons reach the detector in a short instance, resulting in the integrated photon energy being the sum of all received gamma-ray beam energy. Therefore, methods like Compton-scattering[22, 23], photonuclear activation[24, 25], and differential filtering[26, 27] are employed to detect ultra-short gamma-ray flashes. The neutron speration thresholds relevant to the photonuclear activation cover a wide energy range[25], while the attenuation coefficients are not so senstive to gamma energy above 2MeV in diffrential filtering [28]. Thus their spectrum resolutions are limited, especially in the high energy region.

In this experiment, we chose differential filtering detector (DFD) and CSS together to detect these photons. A typical CSS usually uses a uniform magnetic field profile[22] or a stepped magnetic field profile[23] to deflect the photon-induced electron-positron pairs. The latter employs a curved surface plate to improve the energy resolution. Instead, we apply a gradual magnetic field for CSS, which increases linearly along the laser direction and fills the whole spectrometer. Thus, it is capable of gathering the converted electrons with the same energy but different emitting angles together and enhance the energy resolution of the gamma-ray beam as shown in Fig. 1(b). There is the electron-positron pair effect in MeV gamma-ray range. The influence of the electron-positron pair effect can be largely eliminated through their mutual cancellation by the adoption of a symmetrical design for the spectrometer such that the positron and electron spectra are measured simultaneously. Then the energy spectrum of gamma-beams can be obtained from the corrected converted electron energy spectrum. The DFD is placed behind the CSS, which consists of 13 pieces of lead filter with dimensions $2.5\mathrm{cm} \times 2.5\mathrm{cm}$ and different thicknesses in the range of $3-10\mathrm{mm}$, placed one by one in the beam path, as shown in Fig. 1(a). The gamma-ray beam spectrum is calculated using the gamma-ray signal in each IP, considering the lead filter thickness and the attenuation coefficients of these thirteen energy groups. We use equation $\mathrm{D_i} = \Sigma_j^n R_{ij}\Phi_j, i = 1,2,\cdots,13$ to calculated gamma-ray beam spectrum where $\mathrm{D_i}$ represents the energy deposition on the i channel detector, Φ_j is the photon number in the j

https://doi.org/10.1017/hpl.2023.25 Published online by Cambridge University Press

energy interval, n is the number of filters, R_{ij} is the energy deposition coefficient of photons in the j energy interval on the i filter. The CSS and DFD are added 500 mm behind the lead target, which has an acceptance divergence angle of 1.1°. Additionally, the CSS and DFD are shielded by lead box with the thickness of 1 cm and 2cm to avoid the background radiation. Thus, the spectrometers measure the gamma-ray photon signal with low noise.

3. Experimental results and discussion

When a high-intensity $a > 1$ laser pulse with pulse duration τ_p larger than the plasma period λ_p / c propagates through an underdense plasma $n_e < n_c$, it undergoes self-focusing and drives plasma waves through the Raman forward scattering (RFS) and self-modulation instabilities[16]. The gas target is ionized simultaneously and a significant number of electrons are injected and accelerated. In our case, an argon cluster target with high density is employed to enhance the beam charge of energetic electrons from laser-driven electron acceleration[29]. The raw-data recorded by the EPS in Fig. 2(a) shows that the electron bunch has a broad energy spectrum with a cut-off energy of 80 MeV. After the deconvolution[30], the electron spectrum is plotted in Fig. 2(b). The electrons are first accelerated by the longitudinal field, the transverse field leads to betatron-like oscillations of the off-axis electrons. This transverse electric field of the laser, when in near resonance with the betatron motion of the electrons, will in turn increase the transverse momentum of the electrons, which can be converted into longitudinal momentum via the v×B force. This process is analogous to the direct laser acceleration (DLA)[31]. The black line represents the geometric mean value of the data. It is noted that the electrons accelerated in the plasma wave also undergo betatron oscillations about the laser axis due to the restoring force of the ion column that forms behind the drive laser[16]. However most of the radiation from betatron oscillations cannot pass through the thick lead target in the experiment.

https://doi.org/10.1017/hpl.2023.25 Published online by Cambridge University Press

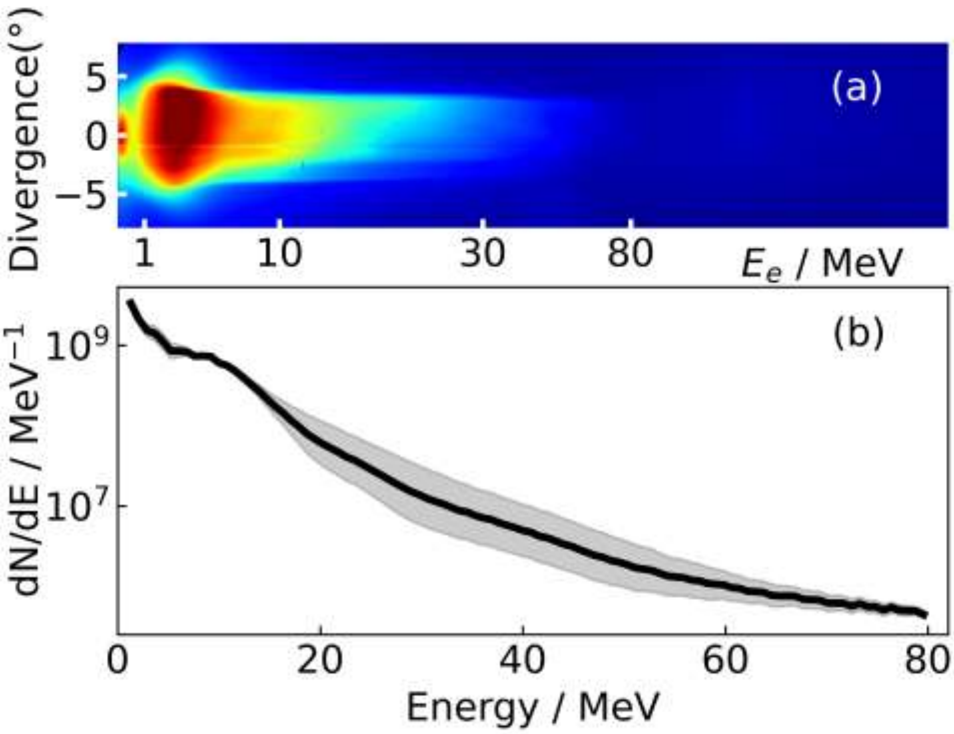

FIG.2. (a) Raw signal of the laser-accelerated electron beam recorded in the IP. (b) Extracted energy spectrum of the energetic electron beam. The black line represents the geometric mean value of the data of two shots. The shaded regions represent uncertainty.

Removing the lead target and spectrometers, a spatial high-energy electron beam analyzer (SHEEBA)[32] composed of Al plates and IPs is located $500\,\mathrm{mm}$ behind the argon target to detect the spatial distribution of electrons. Fig. 3(a) shows a spatial profile of electrons with energy $> 2.2\mathrm{MeV}$, blocked by a 5-mm-thick Al plate in front. It has a Gaussian-type distribution with horizontal divergence of $1.51°$ and vertical divergence of $2.59°$ for shot 4. The spatial distribution of electrons seems to be elliptic, almost the same direction with laser polarization, which could be attributed to the residual transverse momentum[16, 33] that the electrons gain at the moment of ionization and/or to DLA[34, 35]. The divergence angle of electron beam increases while the energy increases from $\mathrm{E} > 9.2\mathrm{MeV}$ to $\mathrm{E} > 15\mathrm{MeV}$, as shown in Fig. 3(b,c). Electron beam divergence angles of 4 continuous shots show good stability in Fig. 3(d), where the blue and red lines indicate the horizontal and vertical divergence angles respectively. An electron beam charge of $26\,\mathrm{nC}$ is measured here, which is beneficial to the subsequent applications. Detailed analysis of the generated electron beams will appear elsewhere. Such high charge electron beams have also been obtained by a picosecond-scale[31] kilojoule-class laser, where the total charge in the electron beams exceeds $700\,\mathrm{nC}$ and scales approximately linearly with laser intensity.

https://doi.org/10.1017/hpl.2023.25 Published online by Cambridge University Press

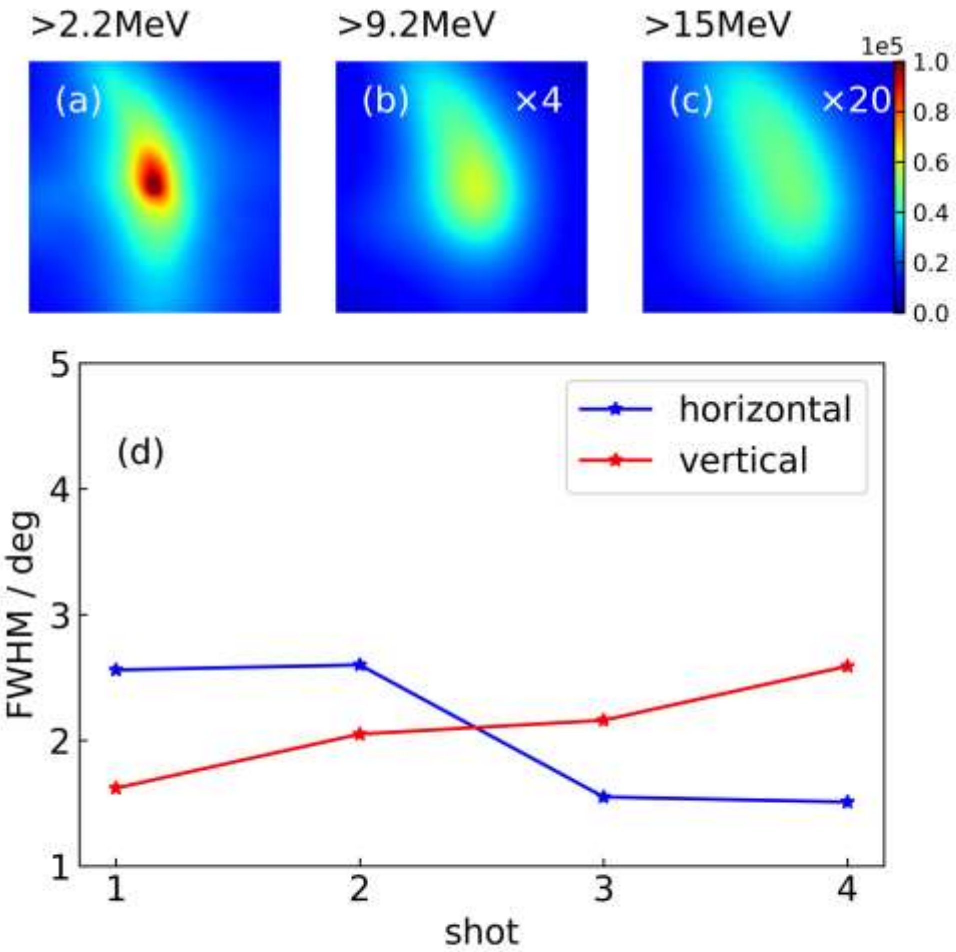

FIG.3. (a-c) Spatial distribution of the electron beam recorded in the IP corresponding to different energies, namely, $E > 2.2$, $E > 9.2$, and $E > 15$MeV. (d) Electron beam divergence angles of 4 continuous shots. The blue and red lines represent horizontal and vertical divergence angles respectively.

These electrons with nC of charge and low divergence then collide with the 2mm thick lead target to generate gamma-ray photons through bremsstrahlung radiation. The EPS serve to remove the secondary electrons and positrons leaving the converting target here. The raw-data recorded by the DFD is shown in Fig. 4(a) within the acceptance angle $1.1°$. The spectrum of gamma-ray beam shows a two-temperature structure (0.6 MeV and 4.4 MeV). It should also be noticed that the gamma-ray signal on the 6th IP is still clear enough after penetrating a 3.8 cm-thick lead-layer. With a 3-mm-thick lead in front of the first IP in Fig. 4(a) to block gamma-ray beams with energy lower than 0.3 MeV, a high total photon number of 2.2×10^9 is detected by the DFD. The raw-data of positrons and electrons recorded by the CSS are shown in Fig. 4(b) and Fig. 4(c). The continuous gamma-ray beam spectrum of geometric mean is shown in Fig. 4(d) by a black line,

https://doi.org/10.1017/hpl.2023.25 Published online by Cambridge University Press

which is in good agreement with the result from the DFD and have a higher energy resolution.

To model the gamma-ray generation process, a series of test particle simulations are carried out with the Monte-Carlo code Geant4[36]. The simulation includes several physical processes such as bremsstrahlung, scattering, ionization, pair production, photoelectric effect and Compton scattering. A total number of 10^7 electrons with the same energy and spatial distributions as the experimental measurement in Fig. 2 and Fig. 3 impact a 2-mm-thick lead target. The electron source is considered point-like. The simulated gamma-ray beam spectrum is shown by the blue line in Fig. 4(d), and it is in good agreement with the experimental result especially in the energy range above $2.5\mathrm{MeV}$. The simulated temperatures of the gamma-ray beam within $1.1°$ are found to be $0.9\mathrm{MeV}$ for low-energy part and $2.7\mathrm{MeV}$ for high-energy part. The slight difference for low-energy part from the experimental result has not been clarified, and further work is needed. Simulations also indicate that the produced gamma-ray source has a FWHM size of $433\mu\mathrm{m}$ at emergent surface of the lead converter.

https://doi.org/10.1017/hpl.2023.25 Published online by Cambridge University Press

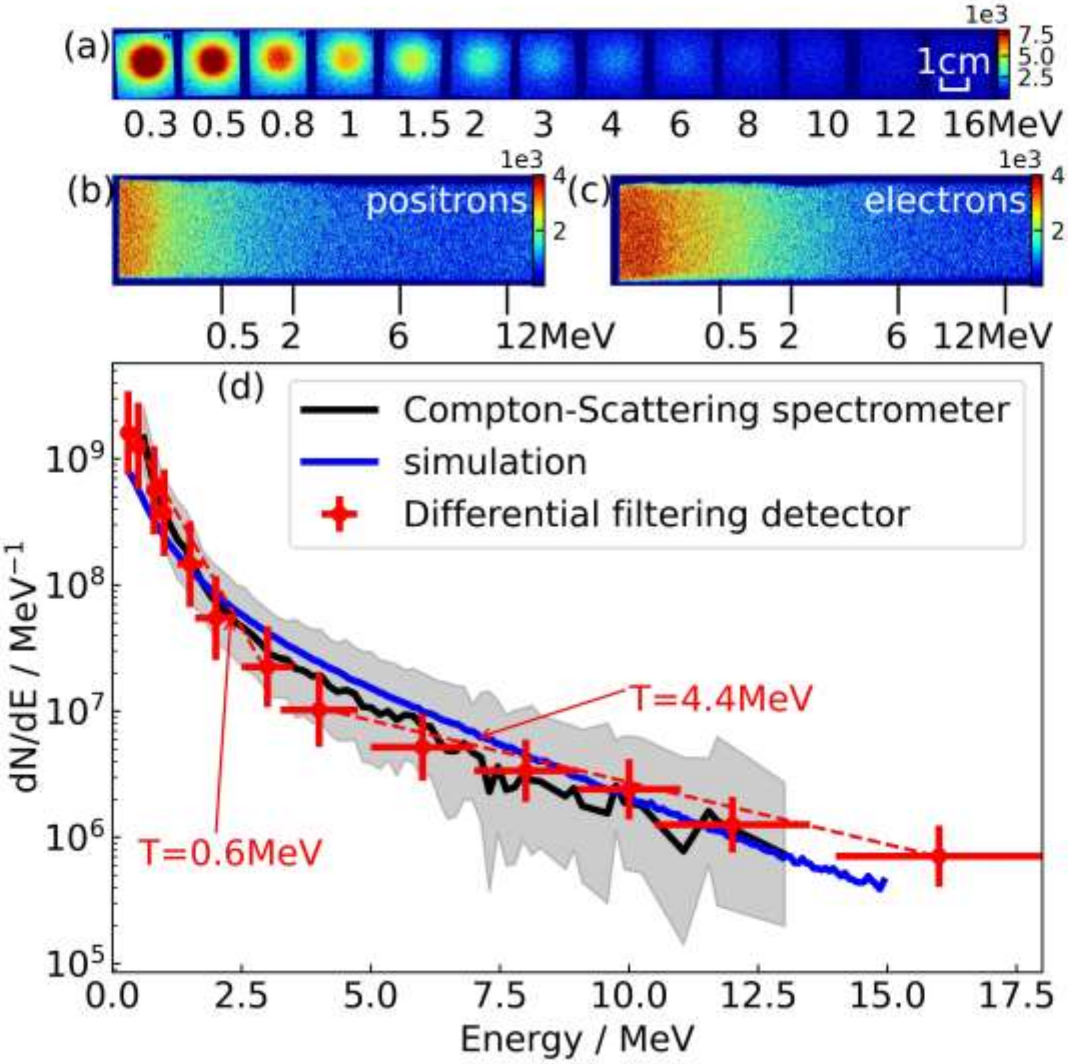

FIG.4. (a) The raw-data of gamma-photon signal recorded by the DFD. The raw-data of positrons (b) and electrons (c) recorded by the CSS. (d) Experimental spectra from the CSS (black solid), the DFD (red cross) , and GEANT4 simulation with the experimental electrons as input (blue solid), within the divergence angle of 1.1°. These horizontal error bars represent thirteen energy intervals and the vertical error bars represent uncertainty for DFD. The black line represents the geometric mean value of the data and the shaded regions represent uncertainty for CSS.

The simulated angular divergence of gamma-ray beam with different energies are summarized in Fig. 5(a). It can be seen that the FWHM divergence of the gamma-ray beam of >0.3MeV is only $7.73°$, which is lower than the recent experimental results under commensurate laser conditions[16]. Considering that the gamma-ray beam has a two-dimensional Gaussian distribution, the acceptance angle of $1.1°$ in the experiment means that only 1% of the photons is measured. Therefore, the total photon number generated in the experiment is estimated to be 2.2×10^{11}-among the highest yield comparing to previous results[16, 17, 37]

https://doi.org/10.1017/hpl.2023.25 Published online by Cambridge University Press

driven by laser-accelerated electrons. It is noted that the gamma-ray photon number could be further increased by raising the picosecond-scale laser energy[31]. The divergence of the gamma-ray beam decreases with the increase of energy as shown in Fig. 5(a). Overall, the gamma-ray beam with high yield and low divergence produced in our experiment could be a promising source for electron-positron production, radiography measurements in HEDS and ICF and nuclear photonics.

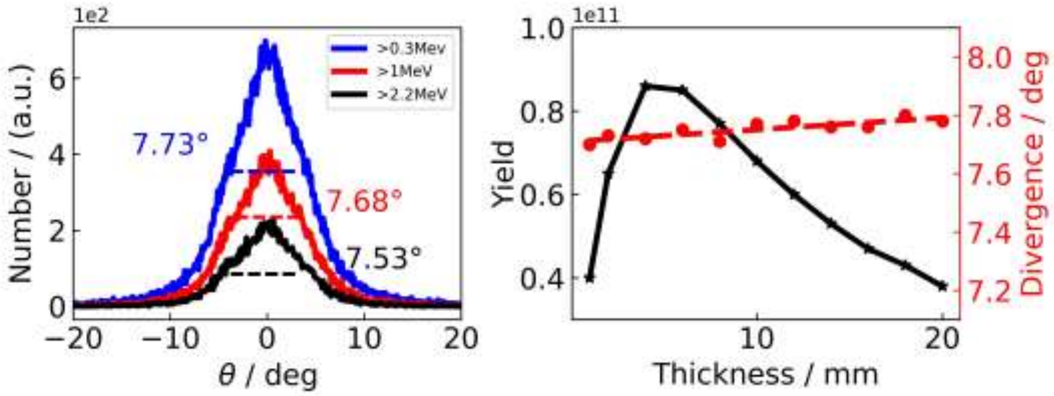

FIG.5. (a) The divergence of gamma-ray beam by GEANT4 simulation with energy > 0.3MeV, > 1MeV and > 2.2MeV. (b) Gamma-ray photon (> 0.3MeV) yields and divergence (FWHM) versus different lead thicknesses. The simulation is performed with the experimental electrons as input.

The influence of thicknesses and FWHM have also been studied by simulation shown in Fig. 5(b). As the target thickness, the generated gamma-ray photon number increases due to continuous interaction between electrons and the target. However, the energetic photons will be attenuated as the target thickness further increases. When these two processes get balance, the largest yield of gamma photons is obtained with the lead target thickness of 4mm. The divergence angle of the gamma-beams is basically unchanged while the target thickness increase.

4. Conclusion

In conclusion, we use a picosecond laser to generate electron beams with large charge and low divergence, and subsequently to generate gamma-ray beams with high yield low divergence through bremsstrahlung radiation. A typical DFD and a special-designed high detection resolution CSS with a gradual magnetic field are used at the same time to detect the generated gamma-ray beams precisely. The gamma-ray beams have a total photon number of 2.2×10^{11}, size of 433μm and divergence of 7.73°, which is promising sources for photonuclear reaction and clinical applications. Future improvements to these sources can be done by using higher laser energies.

https://doi.org/10.1017/hpl.2023.25 Published online by Cambridge University Press

Acknowledgments

This work was supported by the National Natural Science Foundation of China (Grants Nos. 12175299, 11905278, 11975302, 11935008), the CAS Project for Young Scientists in Basic Research (YSBR060) and the Youth Innovation Promotion Association of Chinese Academy of Science (No. 2021242).

REFERENCES

1. A. J. Gonsalves, K. Nakamura, J. Daniels, C. Benedetti, C. Pieronek, T. C. H. de Raadt, S. Steinke, J. H. Bin, S. S. Bulanov, J. van Tilborg, C. G. R. Geddes, C. B. Schroeder, C. Toth, E. Esarey, K. Swanson, L. Fan-Chiang, G. Bagdasarov, N. Bobrova, V. Gasilov, G. Korn, P. Sasorov, and W. P. Leemans, "Petawatt Laser Guiding and Electron Beam Acceleration to 8 GeV in a Laser-Heated Capillary Discharge Waveguide," Physical Review Letters **122**(2019).
2. A. Macchi, M. Borghesi, and M. Passoni, "Ion acceleration by superintense laser-plasma interaction," Reviews of Modern Physics **85**, 751-793 (2013).
3. M. M. Gunther, O. N. Rosmej, P. Tavana, M. Gyrdymov, A. Skobliakov, A. Kantsyrev, S. Zahter, N. G. Borisenko, A. Pukhov, and N. E. Andreev, "Forward-looking insights in laser-generated ultra-intense gamma-ray and neutron sources for nuclear application and science," Nat Commun **13**, 170 (2022).
4. Y. Glinec, J. Faure, L. L. Dain, S. Darbon, T. Hosokai, J. J. Santos, E. Lefebvre, J. P. Rousseau, F. Burgy, B. Mercier, and V. Malka, "High-resolution gamma-ray radiography produced by a laser-plasma driven electron source," Phys Rev Lett **94**, 025003 (2005).
5. A. Giulietti, N. Bourgeois, T. Ceccotti, X. Davoine, S. Dobosz, P. D'Oliveira, M.

Galimberti, J. Galy, A. Gamucci, D. Giulietti, L. A. Gizzi, D. J. Hamilton, E. Lefebvre, L. Labate, J. R. Marques, P. Monot, H. Popescu, F. Reau, G. Sarri, P. Tomassini, and P. Martin, "Intense gamma-ray source in the giant-dipole-resonance range driven by 10-TW laser pulses," Phys Rev Lett **101**, 105002 (2008).

6. X.-B. Wang, G.-Y. Hu, Z.-M. Zhang, Y.-Q. Gu, B. Zhao, Y. Zuo, and J. Zheng, "Gamma-ray generation from ultraintense laser-irradiated solid targets with preplasma," High Power Laser Science and Engineering **8**(2020).

7. G. Sarri, D. J. Corvan, W. Schumaker, J. M. Cole, A. Di Piazza, H. Ahmed, C. Harvey, C. H. Keitel, K. Krushelnick, S. P. Mangles, Z. Najmudin, D. Symes, A. G. Thomas, M. Yeung, Z. Zhao, and M. Zepf, "Ultrahigh Brilliance Multi-MeV gamma-Ray Beams from Nonlinear Relativistic Thomson Scattering," Phys Rev Lett **113**, 224801 (2014).

8. S. Janek, R. Svensson, C. Jonsson, and A. Brahme, "Development of dose delivery verification by PET imaging of photonuclear reactions following high energy photon therapy," Phys Med Biol **51**, 5769-5783 (2006).

9. J. C. Kieffer, A. Krol, Z. Jiang, C. C. Chamberlain, E. Scalzetti, and Z. Ichalalene, "Future of laser-based X-ray sources for medical imaging," Applied Physics B **74**, s75-s81 (2014).

10. G. Breit and J. A. Wheeler, "Collision of Two Light Quanta," Physical Review **46**, 1087-1091 (1934).

11. D. L. Burke, R. C. Field, G. HortonSmith, J. E. Spencer, D. Walz, S. C. Berridge, W. M. Bugg, K. Shmakov, A. W. Weidemann, C. Bula, K. T. McDonald, E. J. Prebys, C. Bamber, S. J. Boege, T. Koffas, T. Kotseroglou, A. C. Melissinos, D. D. Meyerhofer, D.

https://doi.org/10.1017/hpl.2023.25 Published online by Cambridge University Press

A. Reis, and W. Raggk, "Positron production in multiphoton light-by-light scattering," Physical Review Letters **79**, 1626-1629 (1997).

12. T. Nousch, D. Seipt, B. Kämpfer, and A. I. Titov, "Spectral caustics in laser assisted Breit–Wheeler process," Physics Letters B **755**, 162-167 (2016).

13. S. Cipiccia, M. R. Islam, B. Ersfeld, R. P. Shanks, E. Brunetti, G. Vieux, X. Yang, R. C. Issac, S. M. Wiggins, G. H. Welsh, M.-P. Anania, D. Maneuski, R. Montgomery, G. Smith, M. Hoek, D. J. Hamilton, N. R. C. Lemos, D. Symes, P. P. Rajeev, V. O. Shea, J. M. Dias, and D. A. Jaroszynski, "Gamma-rays from harmonically resonant betatron oscillations in a plasma wake," Nature Physics **7**, 867-871 (2011).

14. S. Chen, N. D. Powers, I. Ghebregziabher, C. M. Maharjan, C. Liu, G. Golovin, S. Banerjee, J. Zhang, N. Cunningham, A. Moorti, S. Clarke, S. Pozzi, and D. P. Umstadter, "MeV-Energy X Rays from Inverse Compton Scattering with Laser-Wakefield Accelerated Electrons," Physical Review Letters **110**(2013).

15. K. Ta Phuoc, S. Corde, C. Thaury, V. Malka, A. Tafzi, J. P. Goddet, R. C. Shah, S. Sebban, and A. Rousse, "All-optical Compton gamma-ray source," Nature Photonics **6**, 308-311 (2012).

16. N. Lemos, F. Albert, J. L. Shaw, D. Papp, R. Polanek, P. King, A. L. Milder, K. A. Marsh, A. Pak, B. B. Pollock, B. M. Hegelich, J. D. Moody, J. Park, R. Tommasini, G. J. Williams, H. Chen, and C. Joshi, "Bremsstrahlung hard x-ray source driven by an electron beam from a self-modulated laser wakefield accelerator," Plasma Phys Contr F **60**(2018).

17. S. Li, B. Shen, J. Xu, T. Xu, Y. Yu, J. Li, X. Lu, C. Wang, X. Wang, X. Liang, Y. Leng, R.

https://doi.org/10.1017/hpl.2023.25 Published online by Cambridge University Press

Li, and Z. Xu, "Ultrafast multi-MeV gamma-ray beam produced by laser-accelerated electrons," Physics of Plasmas **24**(2017).

18. S. Corde, K. Ta Phuoc, G. Lambert, R. Fitour, V. Malka, A. Rousse, A. Beck, and E. Lefebvre, "Femtosecond x rays from laser-plasma accelerators," Reviews of Modern Physics **85**, 1-48 (2013).

19. J. Zhu, J. Zhu, X. Li, B. Zhu, W. Ma, X. Lu, W. Fan, Z. Liu, S. Zhou, G. Xu, G. Zhang, X. Xie, L. Yang, J. Wang, X. Ouyang, L. Wang, D. Li, P. Yang, Q. Fan, M. Sun, C. Liu, D. Liu, Y. Zhang, H. Tao, M. Sun, P. Zhu, B. Wang, Z. Jiao, L. Ren, D. Liu, X. Jiao, H. Huang, and Z. Lin, "Status and development of high-power laser facilities at the NLHPLP," High Power Laser Science and Engineering **6**(2018).

20. T. Xu, B. Shen, J. Xu, S. Li, Y. Yu, J. Li, X. Lu, C. Wang, X. Wang, X. Liang, Y. Leng, R. Li, and Z. Xu, "Ultrashort megaelectronvolt positron beam generation based on laser-accelerated electrons," Physics of Plasmas **23**(2016).

21. G. J. Williams, B. R. Maddox, H. Chen, S. Kojima, and M. Millecchia, "Calibration and equivalency analysis of image plate scanners," Rev Sci Instrum **85**, 11E604 (2014).

22. D. J. Corvan, G. Sarri, and M. Zepf, "Design of a compact spectrometer for high-flux MeV gamma-ray beams," Rev Sci Instrum **85**, 065119 (2014).

23. Z.-C. Zhang, T. Yang, G.-Y. Hu, M.-T. Li, W. Luo, N. An, and J. Zheng, "Compact broadband high-resolution Compton spectroscopy for laser-driven high-flux gamma rays," Matter and Radiation at Extremes **6**(2021).

24. W. P. Leemans, D. Rodgers, P. E. Catravas, C. G. R. Geddes, G. Fubiani, E. Esarey, B. A. Shadwick, R. Donahue, and A. Smith, "Gamma-neutron activation experiments

https://doi.org/10.1017/hpl.2023.25 Published online by Cambridge University Press

using laser wakefield accelerators," Physics of Plasmas **8**, 2510-2516 (2001).

25. M. M. Günther, K. Sonnabend, E. Brambrink, K. Vogt, V. Bagnoud, K. Harres, and M. Roth, "A novel nuclear pyrometry for the characterization of high-energy bremsstrahlung and electrons produced in relativistic laser-plasma interactions," Physics of Plasmas **18**(2011).

26. C. D. Chen, J. A. King, M. H. Key, K. U. Akli, F. N. Beg, H. Chen, R. R. Freeman, A. Link, A. J. Mackinnon, A. G. MacPhee, P. K. Patel, M. Porkolab, R. B. Stephens, and L. D. Van Woerkom, "A Bremsstrahlung spectrometer using k-edge and differential filters with image plate dosimeters," Rev Sci Instrum **79**, 10E305 (2008).

27. R. Nolte, R. Behrens, M. Schnurer, A. Rousse, and P. Ambrosi, "A TLD-based few-channel spectrometer for X ray fields with high fluence rates," Radiat Prot Dosim **84**, 367-370 (1999).

28. J. H. Hubbell, H. A. Gimm, and I. O/verbo, "Pair, Triplet, and Total Atomic Cross Sections (and Mass Attenuation Coefficients) for 1 MeV-100 GeV Photons in Elements Z=1 to 100," Journal of Physical and Chemical Reference Data **9**, 1023-1148 (1980).

29. L. M. Chen, W. C. Yan, D. Z. Li, Z. D. Hu, L. Zhang, W. M. Wang, N. Hafz, J. Y. Mao, K. Huang, Y. Ma, J. R. Zhao, J. L. Ma, Y. T. Li, X. Lu, Z. M. Sheng, Z. Y. Wei, J. Gao, and J. Zhang, "Bright betatron X-ray radiation from a laser-driven-clustering gas target," Sci Rep **3**, 1912 (2013).

30. T. Bonnet, M. Comet, D. Denis-Petit, F. Gobet, F. Hannachi, M. Tarisien, M. Versteegen, and M. M. Aleonard, "Response functions of imaging plates to photons,

https://doi.org/10.1017/hpl.2023.25 Published online by Cambridge University Press

electrons and 4He particles," Rev Sci Instrum **84**, 103510 (2013).

31. J. L. Shaw, M. A. Romo-Gonzalez, N. Lemos, P. M. King, G. Bruhaug, K. G. Miller, C. Dorrer, B. Kruschwitz, L. Waxer, G. J. Williams, M. V. Ambat, M. M. McKie, M. D. Sinclair, W. B. Mori, C. Joshi, H. Chen, J. P. Palastro, F. Albert, and D. H. Froula, "Microcoulomb (0.7 +/- [Formula: see text] muC) laser plasma accelerator on OMEGA EP," Sci Rep **11**, 7498 (2021).

32. M. Galimberti, A. Giulietti, D. Giulietti, and L. A. Gizzi, "SHEEBA: A spatial high energy electron beam analyzer," Review of Scientific Instruments **76**(2005).

33. C. Thaury, E. Guillaume, S. Corde, R. Lehe, M. Le Bouteiller, K. Ta Phuoc, X. Davoine, J. M. Rax, A. Rousse, and V. Malka, "Angular-momentum evolution in laser-plasma accelerators," Phys Rev Lett **111**, 135002 (2013).

34. J. L. Shaw, N. Lemos, L. D. Amorim, N. Vafaei-Najafabadi, K. A. Marsh, F. S. Tsung, W. B. Mori, and C. Joshi, "Role of Direct Laser Acceleration of Electrons in a Laser Wakefield Accelerator with Ionization Injection," Phys Rev Lett **118**, 064801 (2017).

35. S. P. Mangles, A. G. Thomas, M. C. Kaluza, O. Lundh, F. Lindau, A. Persson, F. S. Tsung, Z. Najmudin, W. B. Mori, C. G. Wahlstrom, and K. Krushelnick, "Laser-wakefield acceleration of monoenergetic electron beams in the first plasma-wave period," Phys Rev Lett **96**, 215001 (2006).

36. S. Agostinelli and J. Allison and K. Amako and J. Apostolakis and H. Araujo and P. Arce and M. Asai and D. Axen and S. Banerjee and G. Barrand and F. Behner and L. Bellagamba and J. Boudreau and L. Broglia and A. Brunengo and H. Burkhardt and S. Chauvie and J. Chuma and R. Chytracek and G. Cooperman and G. Cosmo and P.

https://doi.org/10.1017/hpl.2023.25 Published online by Cambridge University Press

Degtyarenko and A. Dell'Acqua and G. Depaola and D. Dietrich and R. Enami and A. Feliciello and C. Ferguson and H. Fesefeldt and G. Folger and F. Foppiano and A. Forti and S. Garelli and S. Giani and R. Giannitrapani and D. Gibin and J. J. Gómez Cadenas and I. González and G. Gracia Abril and G. Greeniaus and W. Greiner and V. Grichine and A. Grossheim and S. Guatelli and P. Gumplinger and R. Hamatsu and K. Hashimoto and H. Hasui and A. Heikkinen and A. Howard and V. Ivanchenko and A. Johnson and F. W. Jones and J. Kallenbach and N. Kanaya and M. Kawabata and Y. Kawabata and M. Kawaguti and S. Kelner and P. Kent and A. Kimura and T. Kodama and R. Kokoulin and M. Kossov and H. Kurashige and E. Lamanna and T. Lampén and V. Lara and V. Lefebure and F. Lei and M. Liendl and W. Lockman and F. Longo and S. Magni and M. Maire and E. Medernach and K. Minamimoto and P. Mora de Freitas and Y. Morita and K. Murakami and M. Nagamatu and R. Nartallo and P. Nieminen and T. Nishimura and K. Ohtsubo and M. Okamura and S. O'Neale and Y. Oohata and K. Paech and J. Perl and A. Pfeiffer and M. G. Pia and F. Ranjard and A. Rybin and S. Sadilov and E. Di Salvo and G. Santin and T. Sasaki and N. Savvas and Y. Sawada and S. Scherer and S. Sei and V. Sirotenko and D. Smith and N. Starkov and H. Stoecker and J. Sulkimo and M. Takahata and S. Tanaka and E. Tcherniaev and E. Safai Tehrani and M. Tropeano and P. Truscott and H. Uno and L. Urban and P. Urban and M. Verderi and A. Walkden and W. Wander and H. Weber and J. P. Wellisch and T. Wenaus and D. C. Williams and D. Wright and T. Yamada and H. Yoshida and D. Zschiesche, "Geant4—a simulation toolkit," Nuclear Instruments and Methods in Physics Research Section A: Accelerators, Spectrometers, Detectors and

https://doi.org/10.1017/hpl.2023.25 Published online by Cambridge University Press

Associated Equipment **506**, 250-303 (2003).

37. A. Döpp, E. Guillaume, C. Thaury, A. Lifschitz, F. Sylla, J. P. Goddet, A. Tafzi, G. Iaquanello, T. Lefrou, P. Rousseau, E. Conejero, C. Ruiz, K. Ta Phuoc, and V. Malka, "A bremsstrahlung gamma-ray source based on stable ionization injection of electrons into a laser wakefield accelerator," Nuclear Instruments and Methods in Physics Research Section A: Accelerators, Spectrometers, Detectors and Associated Equipment **830**, 515-519 (2016).

https://doi.org/10.1017/hpl.2023.25 Published online by Cambridge University Press